Engineering Science and Technology, an International Journal 19 (2016) 313–321

HOSTED BY

Contents lists available at ScienceDirect

Engineering Science and Technology, an International Journal

journal homepage: http://www.elsevier.com/locate/jestch

Full Length Article

Melting heat transfer in boundary layer stagnation-point flow of nanofluid toward a stretching sheet with induced magnetic field

B.J. Gireesha [a,b,*], B. Mahanthesh [b,c], I.S. Shivakumara [d], K.M. Eshwarappa [e]

[a] Department of Mechanical Engineering, Cleveland State University, Cleveland, OH 44114, USA
[b] Department of Studies and Research in Mathematics, Kuvempu University, Shankaraghatta, Shimoga 577 451, Karnataka, India
[c] Deparment of Mathematics, AIMS Institutes, Peenya, Bangalore 560058, Karnataka, India
[d] Department of Mathematics, Bangalore University, Karnataka, India
[e] Department of Mathematics, Government Science College, Hassan, Karnataka, India

ARTICLE INFO

Article history:
Received 20 June 2015
Received in revised form
23 July 2015
Accepted 30 July 2015
Available online 9 September 2015

Keywords:
Induced magnetic field
Melting heat transfer
Stagnation-point
Nanofluid
Heat generation/absorption

ABSTRACT

A steady two-dimensional hydromagnetic stagnation-point flow of an electrically conducting nanofluid past a stretching surface with induced magnetic field, melting effect and heat generation/absorption has been analyzed numerically. The model used for the nanofluid incorporates the effects of Brownian motion and thermophoresis. The nonlinear partial differential equations are transformed into ordinary differential equations using suitable similarity transformations, before being solved numerically. Effect of pertinent parameters on different flow fields are determined and discussed in detail through several plots and a table. Obtained numerical results are compared and found to be in good agreement with previously published results in a limiting sense. Further, in the absence of melting and magnetic field effect, the skin friction co-efficient results are compared with exact solutions, which are reported earlier.

1. Introduction

Boundary layer flow and heat transfer characteristics over stretching surfaces have been the topics of extensive research due to their wide range of applications, such as manufacturing of food and paper, polymer extrusion, wire drawing, glass fiber production, stretching of plastic films and many others. Sakiadis [1] was the first among others to consider the steady boundary layer flow of a viscous incompressible fluid on a continuous flat surface. Crane [2] extended this work [1] over a stretching surface. The results obtained in the present study have similar physical agreement with the work of Crane [2] and Hsiao [3,4] who have studied the heat and mass mixed convection for magnetohydro-dynamic viscoelastic fluid past a stretching sheet with Ohmic dissipation. An analysis has been made by Liancun et al. [5] to study the solution of an unsteady flow and heat transfer on a permeable stretching sheet with non uniform heat source/sink. Recently, Gireesha et al. [6] reported the numerical solution for boundary layer flow past a non-isothermal stretching surface with Hall effect. On the other hand, stagnation regions exist on all blunt bodies moving in a viscous fluid. The stagnation-point flow is described as the fluid flow near the stagnation region of a circular body, which exists for both the cases of a fixed or moving body in a fluid. The study of boundary layer stagnation-point flow of an incompressible viscous fluid on a stretching sheet has attracted the attention of researchers due to its wide applications in industry and practical applications. Some of the applications are cooling of electronic devices by fans, cooling of nuclear reactors during emergency shutdown, solar central receivers exposed to wind currents, in the design of thrust bearings and radial diffusers, drag reduction, thermal oil recovery and many hydrodynamic processes. In view of these applications, Hiemenz [7] investigated the two-dimensional stagnation point flow over a plate. Later on, Gorla [8] studied the stagnation point flow of a non-Newtonian fluid in the presence of a transverse magnetic field. Mahapatra and Gupta [9] analyzed heat transfer characteristics in stagnation-point flow toward stretching sheet. Representative studies dealing with the stagnation-point flow have been reported by Nazar et al. [10], Ishak et al. [11], Takhar et al. [12] and Ramesh et al. [13].

Nanofluid is a fluid containing nanometer sized particles, called nanoparticles. It is well known that the nanofluids can tremendously enhance the heat transfer characteristics of the base fluid. Heat transfer is an important process in physics and engineering, and therefore improvements in heat transfer characteristics will improve the efficiency of many processes. Thus, nanofluids have many applications in industry such as heat exchangers, coolants, micro-channel heat sinks and lubricants. Based on these real world applications, Choi [14] has introduced the concept of nanofluid in

* Corresponding author. Tel.: +91 9741148002, fax: +91 08282 256255.
E-mail address: g.bijjanaljayanna@csuohio.edu (B.J. Gireesha).
Peer review under responsibility of Karabuk University.

http://dx.doi.org/10.1016/j.jestch.2015.07.012

order to develop advanced heat transfer fluids with substantially higher conductivities. Later on, the boundary layer flow of nanofluid past a stretching surface under the effect of Brownian motion and thermophoresis was investigated by Khan and Pop [15]. Kuznetsov and Nield [16] investigated the natural convective boundary-layer flow of a nanofluid past a vertical plate by incorporating Brownian motion and thermophoresis effects. Recently, Chamkha et al. [17] analyzed the natural convection past a sphere embedded in a porous medium saturated by a nanofluid. Gorla et al. [18] have reported the numerical solutions for a steady boundary layer flow of nanofluid on a stretching circular cylinder in a stagnant free stream. Unsteady boundary layer stagnation-point flow in a nanofluid was examined by Bachok et al. [19]. Makinde and Aziz [20] obtained the numerical solution for boundary layer flow and heat transfer of nanofluid over a stretching surface with convective boundary conditions. Alsaedi et al. [21] analyzed the stagnation point flow of nanofluid near a permeable stretched surface with convective boundary. A numerical study has been carried out by Gireesha et al. [22] to study the nanoparticle effects on three-dimensional boundary layer flow and heat transfer of an Eyring–Powell fluid over a stretching sheet. They also considered the Brownian motion and thermophoresis effects and solved the problem using Shooting method. Hsiao [23] investigated the heat and mass transfer mixed convection nanofluid flow. Chaoli et al. [24] studied the MHD flow and radiation heat transfer of nanofluids in porous media with variable surface heat flux and chemical reaction. The velocity slip and temperature jump effects on nanofluid over a stretching sheet was carried out by Liancun et al. [25]. Recently, Gireesha et al. [26] have studied the effect of dust particles on boundary layer flow and heat transfer of nanofluid over a porous stretching surface.

Melting heat transfer in steady laminar flow over a stationary flat plate has been studied by Epstein and Cho [27]. Then after, Kazmierczak et al. [28] studied the steady convection flow over a flat plate embedded in a porous medium with melting heat transfer effect. Gorla et al. [29] have studied the melting heat transfer in mixed convection flow over vertical plate. Recently, an analysis has been carried out by Bachok et al. [30] to analyze a steady two-dimensional stagnation point flow and heat transfer over a melting stretching sheet. On the other hand, the effect of an induced magnetic field in an electrically conducting fluid has wide range of applications in real world problems. Such studies are pertinent in astronautical re-entry, thermo-magneto-aerodynamics, nuclear reactors, MHD energy generator systems and magnetohydrodynamic boundary layer control technologies [31]. To date, very little attention has been shown to consider the effect of induced magnetic field on boundary layer flow and heat transfer over surfaces. Kumari et al. [32] considered the boundary layer flow and heat transfer on stretching surface with induced magnetic field. An unsteady laminar boundary layer flow of an electrically conducting fluid past a semi-infinite flat plate with an aligned magnetic field has been studied by Takhar et al. [33]. Beg et al. [34] studied the hydromagnetic convection flow of a Newtonian, electrically-conducting liquid metal past a translating, non-conducting plate with aligned magnetic field. Ghosh et al. [35] presented an exact solution for hydromagnetic natural convection boundary layer flow past an infinite vertical flat plate under the influence of a transverse magnetic field with magnetic induction effects. Liancun et al. [36] have addressed the MHD effects on the flow and heat transfer over a porous shrinking surface with velocity slip and temperature jump. Recently, Ali et al. [37,38] investigated the influence of an induced magnetic field on boundary layer stagnation-point flow over a stretching surface.

Motivated by the aforementioned works, the aim of the present study is to investigate the influence of magnetohydrodynamic effects on melting heat transfer in boundary layer stagnation-point flow of an electrically conducting nanofluid toward a stretching surface with heat source/sink and induced magnetic field. The novelty of this study is to analyze the effect of an induced magnetic field on melting heat transfer in electrically conducting nanofluids. After applying similarity transformations, the resulting governing equations have been solved numerically using standard method called Runge–Kutta–Fehlberg fourth-fifth order scheme for velocity, temperature and concentration profiles.

2. Problem formulation

The physical configuration of the present problem is as shown in Fig. 1. We have considered a steady two-dimensional hydromagnetic boundary layer flow of an electrically conducting nanofluid near a stagnation point toward a stretching surface in its own plane with velocity proportional to the distance from stagnation point. The influence of an induced magnetic field is taken into account.

It is assumed that the velocity of an external flow is $U_e(x)=ax$ and the velocity of stretching sheet is $U_\omega(x)=cx$, where a and c are positive constants. The temperature of melting surface is T_m, while ambient values of temperature and nanoparticle volume fraction are T_∞ and C_∞ respectively, where $T_\infty > T_m$ and C_w is the value of nanoparticle volume fraction at the surface.

The basic equations for the steady flow of an electrically conducting nanofluid by neglecting the effect of Hall current, viscous dissipation and Ohmic heating can be written as follows ([34] and [35]);

Continuity equation for velocity:

$$\nabla\cdot\boldsymbol{V}=0, \tag{2.1a}$$

Continuity equation for induced magnetic field:

$$\nabla\cdot\boldsymbol{H}=0, \tag{2.1b}$$

Conservation of momentum equation:

$$\rho_f(\boldsymbol{V}\cdot\nabla)\mathbf{V}-\frac{\mu_e}{4\pi}(\mathbf{H}\cdot\nabla)\mathbf{H}=-\nabla P+\mu\nabla^2\boldsymbol{V}, \tag{2.2}$$

Conservation of induced magnetic field equation:

$$\nabla\times(\mathbf{V}\times\mathbf{H})+\eta_0\nabla^2\mathbf{H}=0, \tag{2.3}$$

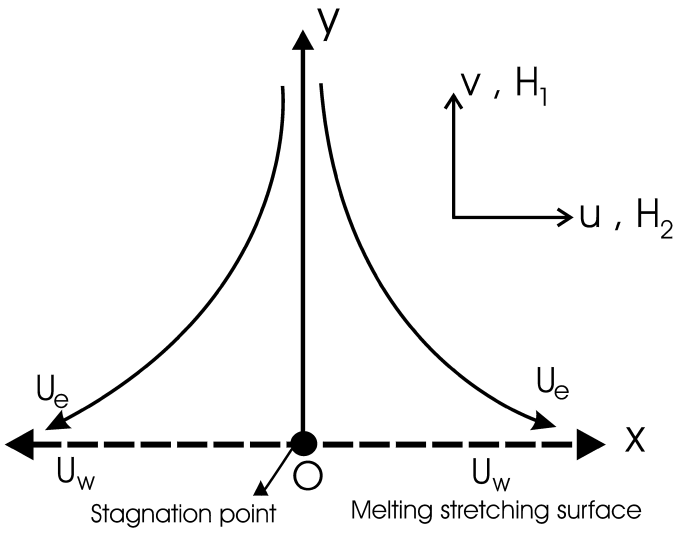

Fig. 1. Physical model and geometry of the problem.

Conservation of energy equation:

$$(\rho c_p)_f(\boldsymbol{V}\cdot\nabla T)=k\nabla^2T+(\rho c_p)_p\left(D_B\nabla C\cdot\nabla T+\left(\frac{D_T}{T_\infty}\right)\nabla T\cdot\nabla T\right)+Q_0(T-T_\infty), \tag{2.4}$$

Conservation of nanoparticle volume equation:

$$(\boldsymbol{V}\cdot\nabla C)=D_B\nabla^2C+\left(\frac{D_T}{T_\infty}\right)\nabla^2T, \tag{2.5}$$

where $V=(u,v)$ – nanofluid velocity vector, $\boldsymbol{H}=(H_1,H_2)$ – induced magnetic field vector, the MHD pressure is $P=p+\frac{\mu_e|H^2|}{8\pi}$, p – nanofluid pressure, T – nanofluid temperature, C – nanoparticle volume fraction, ρ_f and ρ_p are respectively density of base fluid and nanoparticles, μ – dynamic viscosity of the nanofluid, μ_e – magnetic permeability, σ – electric conductivity, $\eta_0=\frac{1}{4\pi\sigma\mu_e}$ – magnetic diffusivity, $(\rho c_p)_f$ and $(\rho c_p)_p$ are heat capacities of nanofluid and nanoparticles respectively, k – the thermal conductivity, D_B – Brownian diffusion coefficient, D_T – thermophoretic diffusion coefficient and Q_0 – heat generation/absorption co-efficient. It is worth to mention that $Q_0>0$ corresponds to internal heat generation and $Q_0<0$ corresponds to internal heat absorption.

Under the boundary layer approximations, the governing equations (2.1)–(2.5) take the following forms (see [34] and [35]);

$$\frac{\partial u}{\partial x}+\frac{\partial v}{\partial y}=0, \tag{2.6a}$$

$$\frac{\partial H_1}{\partial x}+\frac{\partial H_2}{\partial y}=0, \tag{2.6b}$$

$$u\frac{\partial u}{\partial x}+v\frac{\partial u}{\partial y}-\frac{\mu_e}{4\pi\rho_f}\left(H_1\frac{\partial H_1}{\partial x}+H_2\frac{\partial H_1}{\partial y}\right)=\left(u_e\frac{\partial u_e}{\partial x}-\frac{\mu_eH_e}{4\pi\rho_f}\frac{dH_e}{dx}\right)+v\frac{\partial^2u}{\partial y^2}, \tag{2.7}$$

$$u\frac{\partial H_1}{\partial x}+v\frac{\partial H_1}{\partial y}-H_1\frac{\partial u}{\partial x}-H_2\frac{\partial u}{\partial y}=\eta_0\frac{\partial^2H_1}{\partial y^2}, \tag{2.8}$$

$$u\frac{\partial T}{\partial x}+v\frac{\partial T}{\partial y}=\frac{k}{(\rho c_p)_f}\frac{\partial^2T}{\partial y^2}+\frac{Q_0}{(\rho c_p)_f}(T-T_\infty)+\frac{(\rho c_p)_p}{(\rho c_p)_f}\left\{D_B\frac{\partial C}{\partial y}\frac{\partial T}{\partial y}+\frac{D_T}{T_\infty}\left(\frac{\partial T}{\partial y}\right)^2\right\}, \tag{2.9}$$

$$u\frac{\partial C}{\partial x}+v\frac{\partial C}{\partial y}=D_B\frac{\partial^2C}{\partial y^2}+\frac{D_T}{T_\infty}\frac{\partial^2T}{\partial y^2}, \tag{2.10}$$

where (u,v) and (H_1,H_2) are the velocity and magnetic field components along the x and y directions, respectively, whereas $U_e(x)=ax$ and $H_e(x)=xH_0$ are the x-velocity and x-magnetic field at the edge of the boundary layer and H_0 is the uniform vertical magnetic field value at the infinity upstream.

The relevant boundary conditions applicable to the present problem are [30]

$$u=U_w(x),\quad \frac{\partial H_1}{\partial y}=0,\quad H_2=0,\quad T=T_\infty\quad \text{at}\quad y=0$$

$$u=U_e(x),\quad H_1=H_e=0,\quad T=T_m,\quad \text{as}\quad y\to\infty \tag{2.11}$$

$$\text{and}\quad k\left(\frac{\partial T}{\partial y}\right)_{y=0}=\rho f[\lambda^*+c_s(T_m-T_0)]v(x,0),$$

where λ^* is latent heat transfer of the fluid and c_s is heat capacity of solid surface. Melting boundary condition states that the heat conducted to the melting surface is equal to the heat of melting plus the sensible heat required to raise the solid temperature T_0 to its melting temperature T_m [30].

In order to obtain similarity solutions, consider a set of suitable similarity transformations as follows;

$$u=cxf'(\eta),\quad v=-\sqrt{cv}f(\eta),\quad \theta(\eta)=\frac{T-T_\infty}{T_w-T_\infty},\quad \eta=\sqrt{\frac{U_w}{vx}}y, \tag{2.12}$$

$$H_1=H_0xg'(\eta),\quad H_2=-\sqrt{cv}g(\eta),\quad \phi(\eta)=\frac{C-C_\infty}{C_w-C_\infty},$$

Equation (2.6) is identically satisfied on using equation (2.12). Further, equations (2.6) to (2.10) will recast to the following set of ordinary differential equations;

$$f'''(\eta)+f''(\eta)f(\eta)-f'(\eta)^2+\left(\frac{a}{c}\right)^2+\beta\left(g'(\eta)^2-g''(\eta)g(\eta)-1\right)=0 \tag{2.13}$$

$$\lambda g'''(\eta)+g''(\eta)f(\eta)-f'(\eta)g(\eta)=0 \tag{2.14}$$

$$\theta''(\eta)+\Pr(\theta'(\eta)f(\theta)+Q\theta(\eta)+Nb\theta'(\eta)\phi'(\eta)+Nt\left(\theta'(\eta)^2\right)= \tag{2.15}$$

$$\phi''(\eta)+Le\phi'(\eta)f(\eta)+\left(\frac{N_t}{N_b}\right)\theta''(\eta)=0, \tag{2.16}$$

where a prime denotes differentiation with respect to η, $\beta=\frac{\mu_e}{4\pi\rho_f}\left(\frac{H_0}{c}\right)^2$ is the magnetic parameter, $\lambda=\frac{\eta_0}{v}$ is reciprocal of the magnetic Prandtl number, $Pr=\frac{\mu c_{p_f}}{k}$ is the Prandtl number, $\frac{a}{c}$ is the stretching parameter, $Q=\frac{Q_0}{c(\rho c_p)_f}$ is the heat source/sink parameter, $Nb=\frac{\tau D_B(\phi_w-\phi_\infty)}{v}$ is the Brownian motion parameter, $\tau=\frac{(\rho c_p)_p}{(\rho c_p)_f}$ is the ratio between effective heat capacity of the nanoparticle material and heat capacity of the fluid, $Nt=\frac{\tau D_B(T_w-T_\infty)}{T_\infty v}$ is the thermophoresis parameter and $Le=\frac{v}{D_B}$ is the Lewis number.

Substituting equation (2.12) into the boundary conditions (2.11), one can get;

$$f'(0)=1,\quad g'(0)=0,\quad g(0)=0,\quad Prf(0)+M\theta'(0)=0,\quad \theta(0)=0,$$
$$\phi(0)=1,\quad f'(\infty)\to a/c,\quad g'(\infty)\to1,\quad \theta(\infty)\to1,\quad \phi(\infty)\to1, \tag{2.17}$$

where $M=\frac{c_f(T_\infty-T_w)}{\lambda^*+c_s(T_m-T_0)}$ is the melting parameter.

From the engineering point of view, the physical quantities of interest are local skin friction coefficient C_f, local Nusselt number Nu_x or melting rate at the stretching surface and local Sherwood number Sh_x. The skin friction drag is defined as;

$$C_f=\frac{\tau_w}{\rho_fU_w^2}, \tag{2.18a}$$

The Nusselt number is the dimensionless heat transfer coefficient and can be defined as the ratio of convective and conductive heat transfer rates, i.e.,

$$Nu_x=\frac{xq_w}{k(T_\infty-T_m)}, \tag{2.18b}$$

On the other hand, the Sherwood number is defined as the ratio of convective and diffusive mass transfer rates along a surface and is given by;

$$Sh_x = \frac{x j_w}{D_B(C_w - C_\infty)}, \tag{2.18c}$$

where τ_w, q_w and j_w are the surface shear stress, surface heat flux and surface mass flux respectively, which are given by;

$$\tau_w = \mu\left(\frac{\partial u}{\partial y}\right)_{y=0}, \quad q_w = -k\left(\frac{\partial T}{\partial y}\right)_{y=0}, \quad j_w = -D_B\left(\frac{\partial C}{\partial y}\right)_{y=0} \tag{2.19}$$

Using equation (2.19) and with the aid of similarity variables, we obtain

$$Re_x^{\frac{1}{2}} C_f = f''(0), \quad Re_x^{\frac{1}{2}} Nu_x = -\theta'(0), \quad Re_x^{\frac{1}{2}} Sh = -\phi'(0), \tag{2.20}$$

where $Re_x = \frac{U_w x}{\nu}$ is the local Reynolds number.

It is worth to mention that, in the absence of melting and induced magnetic effects, equation (2.13) with respect to boundary conditions (2.17) is reduced to that of Crane [2]. Crane reported the closed form solution as follows;

$$f(\eta) = 1 - e^{\eta}.$$

Therefore numerical results of the present study obtained for $f'(0)$ when $M = \beta = 0$ is a unique value namely −1.0000 and this is in excellent agreement with that of Crane [2].

3. Numerical method and validation

The systems of nonlinear differential equations (2.13)–(2.16) along with the boundary condition (2.17) are solved numerically using fourth-fifth order Runge–Kutta–Fehlberg method. The absolute convergence criteria were taken as 10^{-6} in this method. It is most important to choose the appropriate finite values of η_∞. The asymptotic boundary conditions at η_∞ were replaced by η_{10} in accordance with standard practice in the boundary layer analysis. The choice of $\eta_\infty = 10$ ensures that all numerical solutions approach the asymptotic values correctly. The present results of dimensionless skin friction co-efficient for different values of a/c in the absence of melting and induced magnetic field effects are compared with those reported by Mahapatra and Gupta [9], Ishak et al. [11], Nazar et al. [10] and Ali et al. [37] in Table 1. It is observed that the comparison shows good agreement for each value considered. Therefore, we are confident that the present results are correct and accurate.

Table 1
Comparison of results for skin friction co-efficient $f'(0)$ in the case of $M = \beta = 0$ for different value of a/c.

a/c	Mahapatra and Gupta [9]	Ishak et al. [11]	Nazar et al. [10]	Ali et al. [37]	Present study
0.1	−0.9694	−0.9694	−0.9694	−0.9694	−0.96938
0.2	−0.9181	−0.9181	−0.9181	−0.9181	−0.91810
0.5	−0.6673	−0.6673	−0.6673	−0.6673	−0.66723
0.5	–	–	–	–	0.90852
2.0	2.0175	2.0175	2.0176	2.0175	2.01750
3.0	4.7293	4.7294	4.7296	4.7293	4.72928
4.0	–	–	–	–	8.00043

4. Results and discussion

The boundary layer flow and melting heat transfer of nanofluid over a stretching sheet in the presence of heat source/sink and induced magnetic field has been investigated numerically. Our main attention is to examine the influence of nanoparticles with an induced magnetic field on the fluid flow near a stagnation-point over a stretching surface. The numerical solutions are presented through graphs 2–19 for the physical interpretation of the proposed study. These figures describe the effect of the magnetic field (β), reciprocal of the magnetic Prandtl number (λ), stretching parameter (a/c), heat source/sink parameter (Q), Brownian motion parameter (Nb), thermophoresis parameter (Nt), Lewis number (Le) and melting parameter (M) on the dimensionless velocity, induced magnetic field, temperature and nanoparticle volume fraction profiles. Further, numerical results of the skin-friction coefficient, Nusselt number, and the Sherwood number are presented in Table 2.

Figs. 2–5 are plotted to show the variations of velocity, induced magnetic field, temperature and nanoparticle fraction profiles within the boundary layer for different values of β, respectively. It is evident from these figures that, all curves approach the far field boundary conditions asymptotically. Further, the velocity, induced magnetic field and temperature profiles increase as β increases for the case $a/c = 0.5$, whereas it shows the reverse effect for the nanoparticle volume fraction profiles for $a/c = 0.5$. However, the whole trend is opposite for the case $a/c = 1.4$.

The effect of melting parameter on velocity, induced magnetic field, temperature and nanoparticle volume fraction profiles for $a/c = 0.5$ and 1.5 are plotted in Figs. 6–9 respectively. It is found from the plots 6 and 7 that, for $a/c = 0.5$, the velocity and induced magnetic field profile increases by increasing M, while it shows the reverse effect for $a/c = 1.5$. It is revealed from Figs. 8 and 9 that the thermal boundary layer becomes steeper for higher value of melting parameter in both $a/c = 0.5$ and $a/c = 1.5$ cases. This result makes sense physically, if it is realized that the melting phenomenon acts as a blowing boundary condition at the stretching surface. Consequently, more intense melting leads to retardation in the thermal boundary layer thickness. These results are consistent with the results obtained by Bachok et al. [24]. However, this effect is reverse for nanoparticle volume fraction profiles as can be seen in Figs. 8 and 9.

Table 2
Numerical values of $f''0), -\theta'(0)$ and $-\phi'(0)$ for different values of $\beta, \lambda, M, Nt, Le, Q$ and a/c.

β	λ	M	Nb	Nt	Le	Q	a/c	$f'(0)$	$-\theta'(0)$	$-\phi'(0)$
0.1	10	1.0	0.5	0.5	1.0	−0.02	0.5	−0.5074	−0.3415	0.5083
0.5								−0.1911	−0.3807	0.5347
1.0								0.1107	−0.4099	0.5560
0.1	100							−0.5473	−0.3359	0.5044
	1000							−0.5523	−0.3351	0.5039
	5000							−0.5527	−0.3351	0.5039
0.1	10	0.0						−0.6297	−0.5088	0.9358
		2.0						−0.4488	−0.2646	0.3284
		4.0						−0.3867	−0.1880	0.1688
0.1	10	1.0	0.1					−0.4947	−0.3806	0.9124
			1.0					−0.5233	−0.2939	0.4880
			1.5					−0.5387	−0.2486	0.5034
0.1	10	1.0	0.5	0.1				−0.5157	−0.3164	0.4614
				1.0				−0.4964	−0.3754	0.6016
				2.0				−0.4723	−0.4515	0.9263
0.1	10	1.0	0.5	0.5	0.1			−0.5036	−0.3533	0.3907
					0.6			−0.5064	−0.3446	0.4753
					1.2			−0.4925	−0.3876	0.6803
0.1	10	1.0	0.5	0.5	1.0	−0.1		−0.5164	−0.3143	0.6487
						0.0		−0.4848	−0.4118	0.6502
						+0.1		−0.4427	−0.5497	0.6315
0.1	10	1.0	0.5	0.5	1.0	0.02	0.5	−0.5074	−0.3415	0.5083
							3.0	3.8695	−0.5905	0.1094

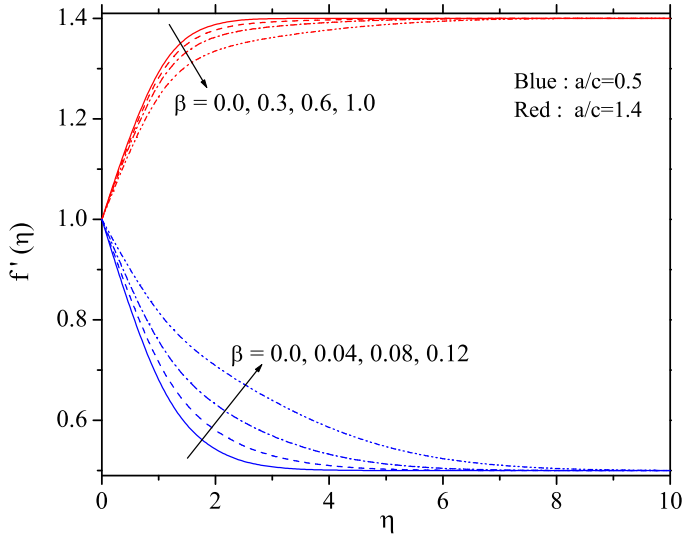

Fig. 2. Effect of β on $f'(\eta)$ profiles in both $a/c = 0.5$ and $a/c = 1.4$ with $\lambda = 5$, $Le = M = 1$, $Nb = Nt = 0.5$, $Pr = 1$, $Q = 0.1$.

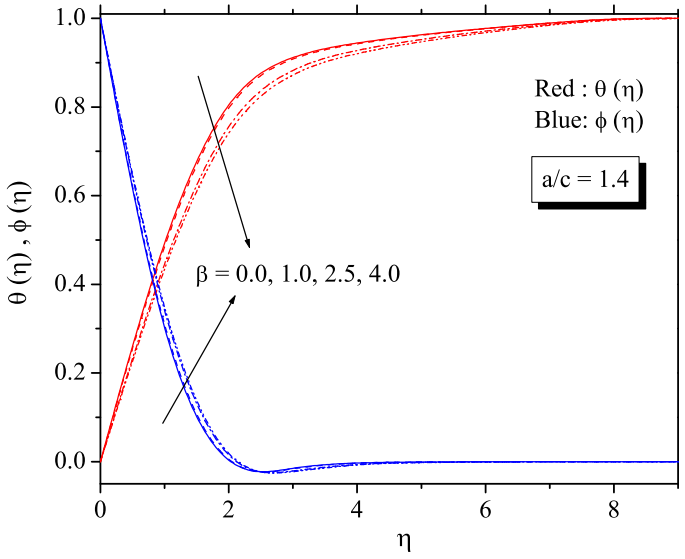

Fig. 4. Effect of β on $\theta(\eta)$ and $\phi(\eta)$ profiles for $a/c = 1.4$ with $\lambda = 5$, $Le = M = 1$, $Nb = Nt = 0.5$, $Pr = 1$, $Q = 0.1$.

Fig. 10(a) and (b) presents the influence of λ on both $f'(\eta)$ and $g'(\eta)$ profiles against span-wise coordinate η with $a/c = 0.5$ respectively. Fig. 10(a) explores that an increase in λ brings a decrease in the momentum boundary layer thickness due to increase in skin friction coefficient $f''(0)$. It is observed from plot 10(b) that $g'(\eta)$ profile decreases near the boundary and increases far away with increase in λ. The dimensionless $\theta(\eta)$ and $\phi(\eta)$ profiles for $a/c = 0.5$ and various values of λ can be displayed in Fig. 11. It shows that an increase in λ causes decrease in the fluid temperature $\theta(\eta)$ within the boundary layer, and consequently the thermal boundary layer thickness decreases. But this trend is opposite for $\phi(\eta)$ profiles.

The effect of stretching parameter a/c on $f'(\eta)$ and $g'(\eta)$, and $\phi(\eta)$ and $\theta(\eta)$ distributions are respectively demonstrated in Figs. 12 and 13. The velocity $f'(\eta)$ profile is found to increase with increase in a/c. The central reason for this effect is, for a fixed value of a/c corresponding to the stretching of the surface, the increase in a in relation to c implies an increase in the straining motion near the stagnation region that can increase the acceleration of the external stream. Therefore, an increase in a/c has the effect of thickening the boundary layer. Nevertheless, inverted boundary layer structure occurs for the flow when $a/c < 1$, where the stretching velocity cx of the surface exceeds the velocity ax of the external stream. From Fig. 12, it can also be noted that the magnetic field profile $g'(\eta)$ decreases as a/c increases. From Fig. 13, it is seen that the temperature profile $\theta(\eta)$ significantly increases with increasing a/c. Further observation shows that as a/c increases, nanoparticle volume fraction profile $\phi(\eta)$ retards rapidly; however, the opposite trend occurs after a certain point.

The effect of Nb on $f'(\eta)$ and $g'(\eta)$ is presented in Fig. 14. It reveals that both velocity and induced magnetic field profile rapidly decrease throughout the boundary layer region for increasing values of Nb. The influence of Nb notably increases $\phi(\eta)$ profile and decreases the $\theta(\eta)$ profile, which is as shown in Fig. 15.

Fig. 16 has been plotted to display the effect of Nt on $g'(\eta)$ and $\theta(\eta)$ distributions by fixing all other parameters. It elucidates that

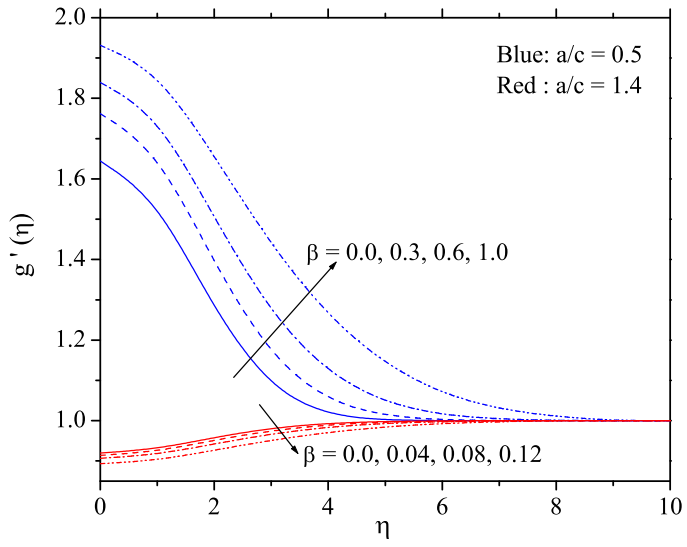

Fig. 3. Effect of β on $g'(\eta)$ profiles in both $a/c = 0.5$ and $a/c = 1.4$ with $\lambda = 5$, $Le = M = 1$, $Nb = Nt = 0.5$, $Pr = 1$, $Q = 0.1$.

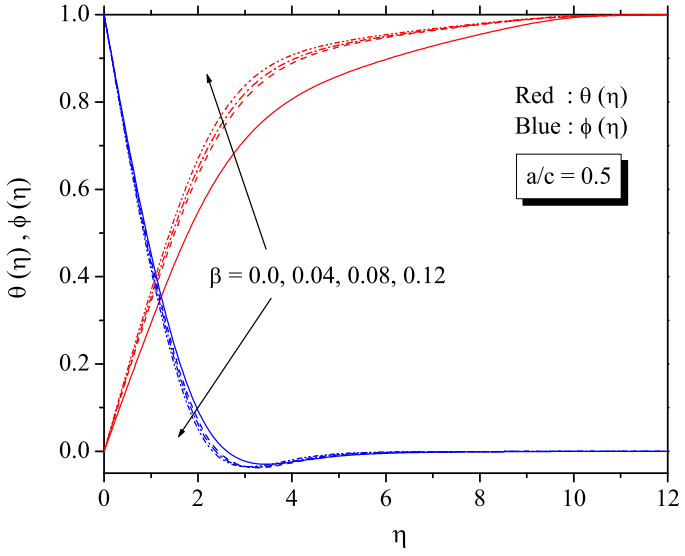

Fig. 5. Effect of β on $\theta(\eta)$ and $\phi(\eta)$ profile for $a/c = 0.5$ with $\lambda = 5$, $Le = M = 1$, $Nb = Nt = 0.5$, $Pr = 1$, $Q = 0.1$.

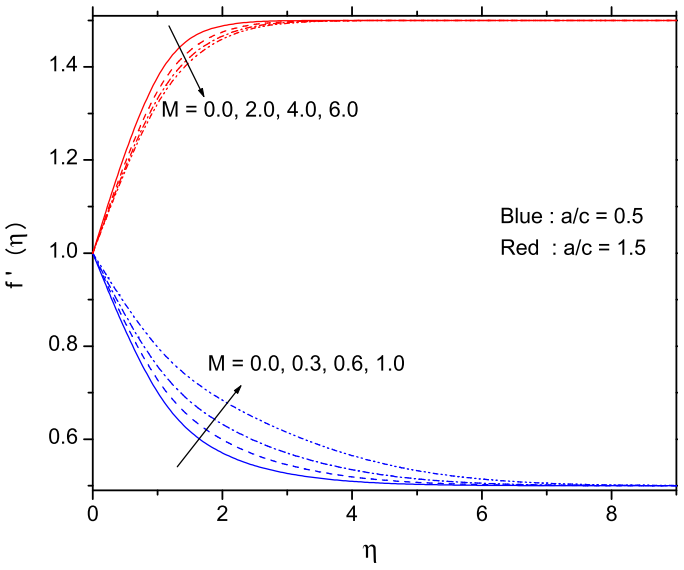

Fig. 6. Effect of M on $f'(\eta)$ profile in both $a/c = 0.5$ and $a/c = 1.5$ with $\beta = 0.1, \lambda = 5, Le = 1, Nb = Nt = 0.5, Pr = 0.72, Q = -0.1$.

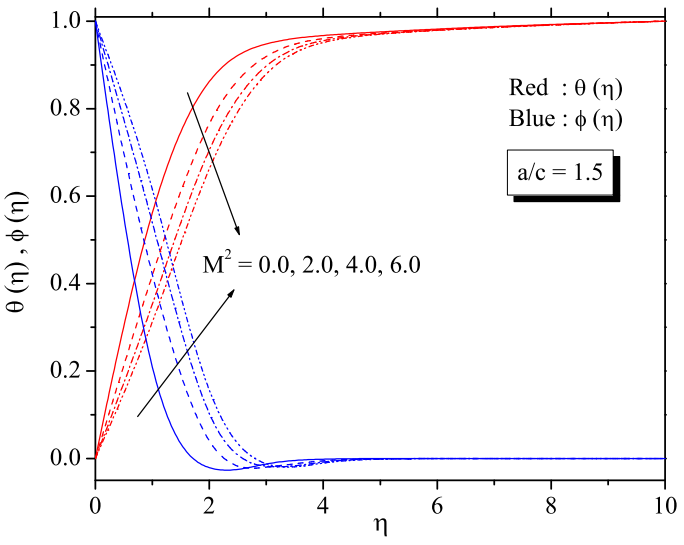

Fig. 8. Effect of M on $\theta(\eta)$ and $\phi(\eta)$ profiles for $a/c = 1.5$ with $\beta = 0.1, \lambda = 5, Le = 1, Nb = Nt = 0.5, Pr = 0.72, Q = -0.1$.

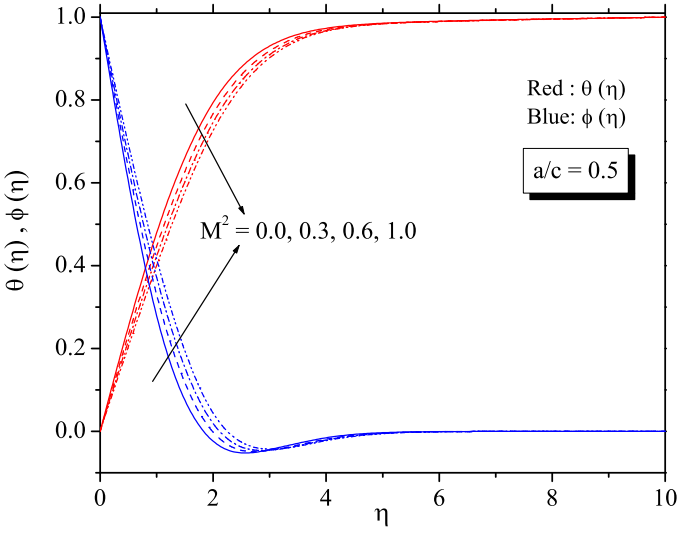

Fig. 9. Effect of M on $\theta(\eta)$ and $\phi(\eta)$ profiles for $a/c = 0.5$ with $\beta = 0.1, \lambda = 5, Le = 1, Nb = Nt = 0.5, Pr = 0.72, Q = -0.1$.

the temperature and induced magnetic field profile shows the same behavior against the value of Nt. The temperature profile as well as the induced magnetic field profile increases with an increase in Nt. Finally, Fig. 17 illustrates the effect of Q on temperature profile and the effect of Le on nanoparticle volume fraction profile versus η. It is seen that increasing values of Q result in increase of temperature profiles along with the thermal boundary layer thickness. It is also observed that $\phi(\eta)$ profile at some point is found to decrease initially with increasing Le, but for large values of η it increases notably with Le. It is quite obvious becauseLe is inversely proportional to diffusion co-efficient. Thus, increasing Le results in decrease on diffusion which finally yields into a decrease of nanoparticle volume faction.

Table 2 was made in order to see the variation of skin-friction coefficient, Nusselt number and volume fraction Sherwood number for different values $\beta, \lambda, M, Nb, Nt, Le, Q$ and a/c. It is found that the skin-friction coefficient increases with an increase in β, M, Nt, Le, Q and a/c and found to be decreasing for increasing values of λ and

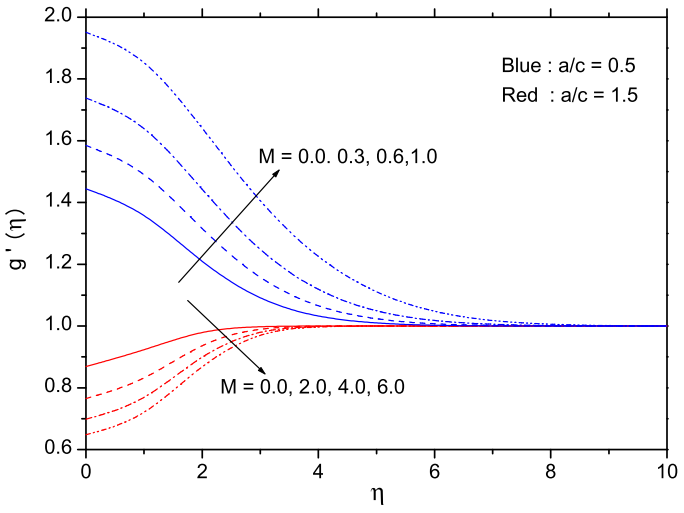

Fig. 7. Effect of M on $g'(\eta)$ profile in both $a/c = 0.5$ and $a/c = 1.5$ with $\beta = 0.1, \lambda = 5, Le = 1, Nb = Nt = 0.5, Pr = 0.72, Q = -0.1$.

Nb. It is observed that the Nusselt number profile enhances for increasing values of λ, M, Nb, and retards with increase in $\beta, Nt, Le, Q, a/c$. In addition, increasing values of λ, M, Nb, cause enhancement in volume fraction Sherwood number profile and an opposite trend is observed with increase in $\lambda, M, Nb, Q, a/c$.

5. Concluding remarks

Using Runge–Kutta–Fehlberg method, the governing equations of the flow have been solved numerically. Our results with limiting cases are compared with previously published results and an excellent agreement is found. The inclusions of nanoparticles into the base fluid of this problem change the flow pattern. It is found that the induced magnetic field and temperature distributions are enhanced with strengthening of the hydromagnetic field. The melting effect is more suited for cooling processes, since the melting effect reduces the temperature of the fluid. It is also found that suspended nanoparticles in a fluid are capable of increasing the heat

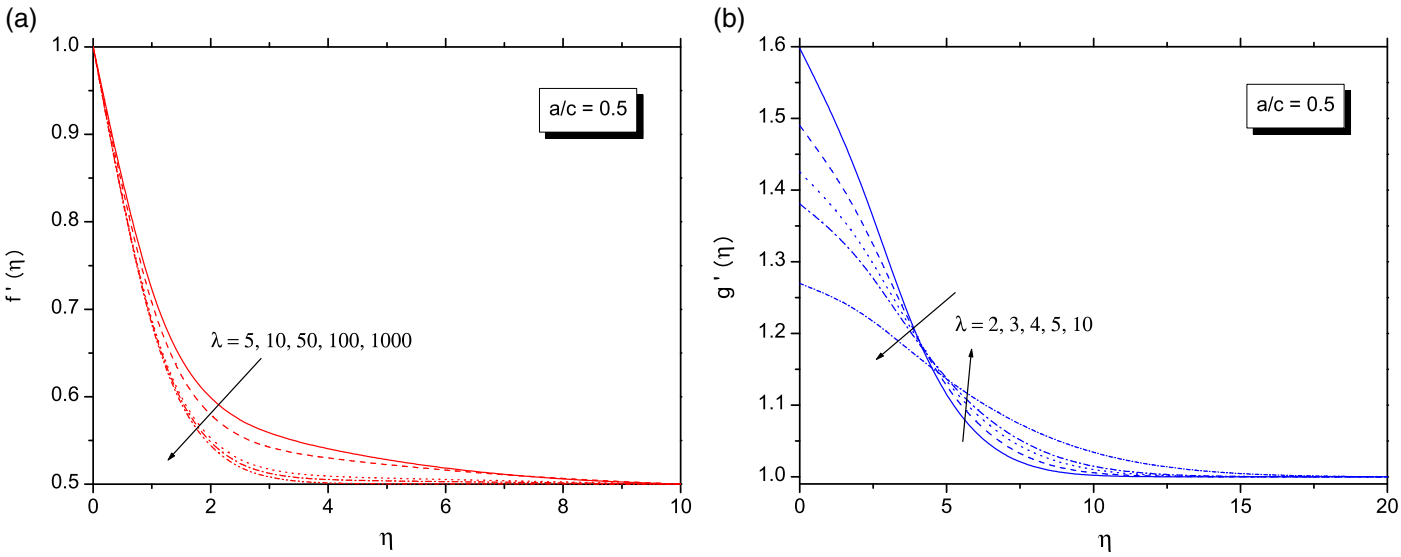

Fig. 10. (a) Effect of λ on $f'(\eta)$ profile for $a/c = 0.5$ with $\beta = 0.1, \lambda = 5, Le = M = 1, Nb = Nt = 0.5, Pr = 0.72, Q = -0.1$. (b) Effect of λ on $g'(\eta)$ profile for $a/c = 0.5$ with $\beta = 0.1, \lambda = 5, Le = M = 1, Nb = Nt = 0.5, Pr = 0.72, Q = -0.1$.

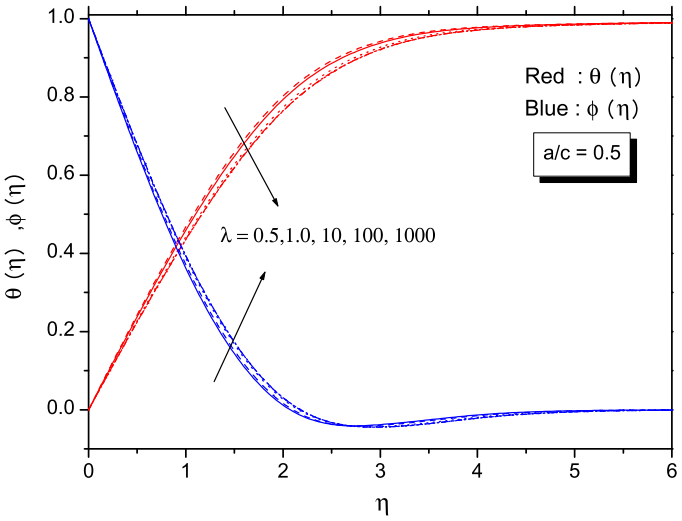

Fig. 11. Effect of λ on $\theta(\eta)$ and $\phi(\eta)$ profiles for $a/c = 0.5$ with $\beta = 0.1, \lambda = 5, Le = M = 1, Nb = Nt = 0.5, Pr = 0.72, Q = -0.1$.

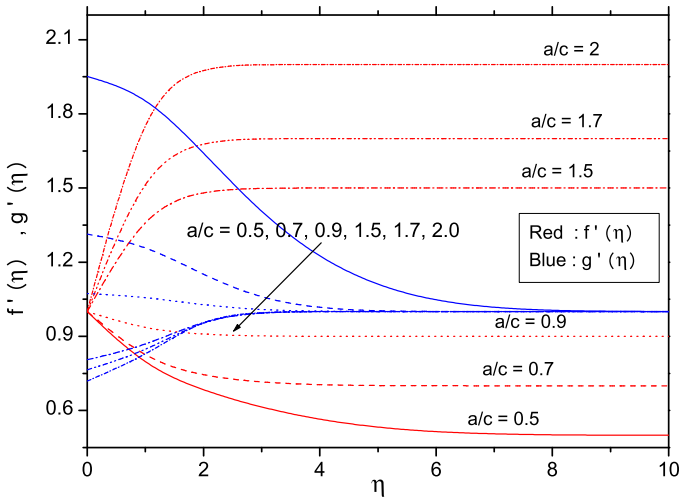

Fig. 12. Effect of a/c on $f'(\eta)$ and $g'(\eta)$, profiles respectively with $\beta = 0.1, \lambda = 5, Le = M = 1, Nb = Nt = 0.5, Pr = 0.72, Q = -0.1$.

transfer capability of the base fluid. Therefore, the nanofluids are preferable in scientific processes that take place at high temperatures, i.e., cooling of a metal or glass sheet. Besides, it is found that the induced magnetic field profiles are affected by nanofluid key parameters such as thermophoresis and Brownian motion parameter. Additionally, the influence of thermophoresis and stretching ratio is to increase the heat transfer rate at the surface. Moreover, the surface heat transfer can be considerably enhanced using a higher melting effect and Brownian motion of nanoparticles. The skin friction drag is lower for $\varepsilon < 1$ when compared with that for $\varepsilon > 1$. Further, under certain conditions, heat addition or absorption is possible. This would be suitable in many engineering and scientific applications. Finally, we can conclude that, the results of the present study are useful in many industrial applications such as heat exchangers, coolants, micro-channel heat sinks and lubricants.

Acknowledgment

The authors wish to express their deep sense of gratitude to the reviewers of the original manuscript for their kind suggestions based upon which the present version of the paper has been prepared. The author B.J. Gireesha wishes to express his gratitude to University Grants Commission [No. F 5-110/2014 (IC)], New Delhi, India for the financial support under Raman Fellowship 2014–2015 for pursuing this work.

Nomenclature

a, c	Constants
a/c	Stretching ratio parameter
c_s	Heat capacity of the solid surface
C	Nanoparticle volume fraction (kg/m^3)
C_w	Concentration at the wall (kg/m^3)
C_∞	Ambient nanofluid volume fraction (kg/m^3)
C_f	Local skin-friction co-efficient
$(c_p)_f$	Specific heat coefficient of fluid $(J/kg\ K)$
$(c_p)_p$	Specific heat coefficient of nanoparticles $(J/kg\ K)$
D_B	Brownian diffusion coefficient
D_T	Thermophoretic diffusion coefficient

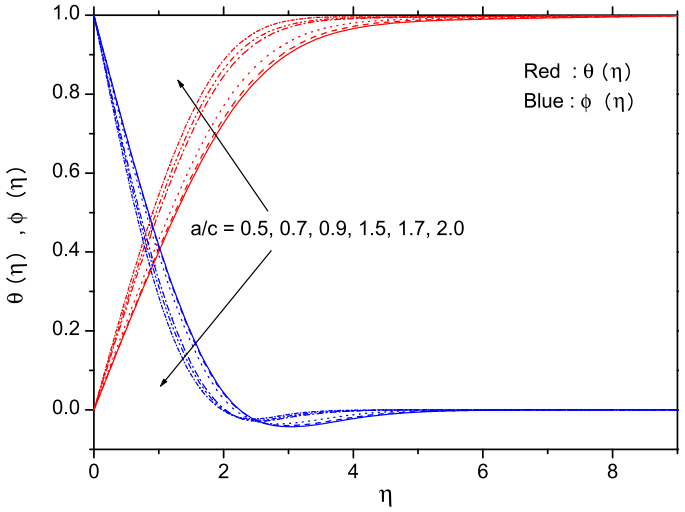

Fig. 13. Effect of a/c on $\theta(\eta)$ and $\phi(\eta)$ profiles respectively with $\beta = 0.1$, $\lambda = 5$, $Le = M = 1$, $Nb = Nt = 0.5$, $Pr = 0.72$, $Q = -0.1$.

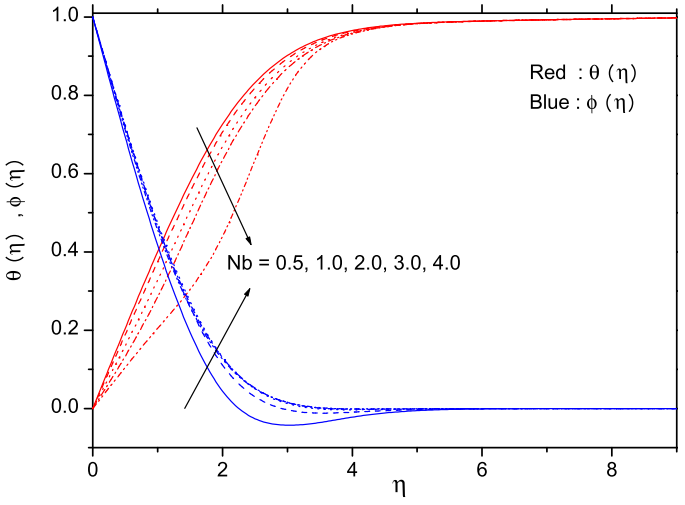

Fig. 15. Effect of Nb on $\theta(\eta)$ and $\phi(\eta)$ profiles for $a/c = 0.5$ with $\beta = 0.1$, $\lambda = Le = M = 1$, $Nb = Nt = 0.5$, $Pr = 0.72$, $Q = -0.1$.

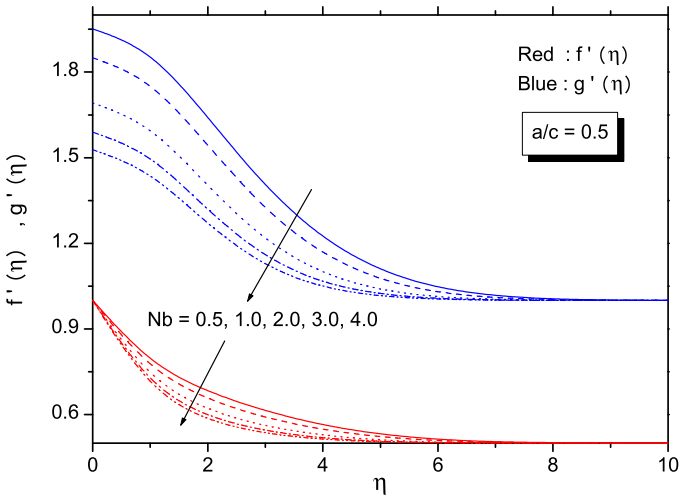

Fig. 14. Effect of Nb on $f'(\eta)$ and $g'(\eta)$ profiles for $a/c = 0.5$ with $\beta = 0.1$, $\lambda = Le = M = 1$, $Nb = Nt = 0.5$, $Pr = 0.72$, $Q = -0.1$.

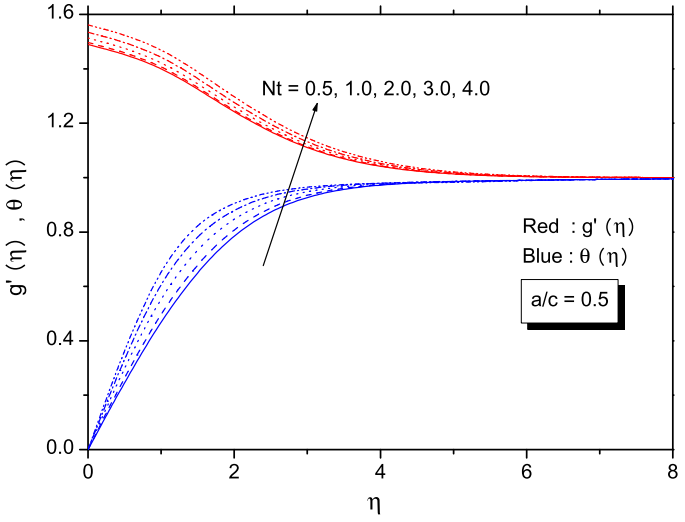

Fig. 16. Effect of Nt on $g'(\eta)$ and $\theta(\eta)$ profiles for $a/c = 0.5$ with $\beta = 0.1$, $\lambda = Le = 1$, $M = 0.1$ $Nb = Nt = 0.5$, $Pr = 0.72$, $Q = -0.1$.

f, g	Dimensionless Velocity and magnetic fields
$\boldsymbol{H}$	Induced magnetic field vector
$H_e(x)$	Magnetic field at the boundary layer edge
H_1, H_2	Magnetic components along x and y directions
H_0	Uniform vertical magnetic field value at the infinity stream
j_w	Nanoparticles mass flux
k	Thermal conductivity ($W/m\ K$)
Le	Lewis number
M	Melting parameter
Nb	Brownian motion parameter
Nt	Thermophoresis parameter
Nu_x	Local Nusselt number
O	Origin
p	Nanofluid Pressure
P	MHD Pressure
Pr	Prandtl number
Q	Heat source/sink parameter
Q_0	Volumetric rate of heat generation or Absorption
q_w	Surface heat flux
Re_x	Local Reynolds number
Sh_x	Sherwood number
T	Fluid temperature (K)
T_m	Melting surface temperature (K)
T_0	Solid surface temperature (K)
T_∞	Ambient Surface temperature (K)
V	Velocity field ($m\ s^{-1}$)
$U_e(x)$	Velocity of the external flow ($m\ s^{-1}$)
$U_w(x)$	Velocity of the stretching sheet ($m\ s^{-1}$)
$u, v,$	Velocity components along x and y directions ($m\ s^{-1}$)
x, y	Coordinates (m)

Greek symbols

θ	Dimensionless temperature
ϕ	Dimensionless nanoparticle volume fraction
ν	Kinematic viscosity of the fluid ($m^2 s^{-1}$)
α_m	Thermal diffusivity
β	Magnetic parameter
μ	Dynamic viscosity ($kg\ m^{-1}\ s^{-1}$)
μ_e	Magnetic permeability ($kg\ m^{-1}\ s^{-1}$)
σ	Electric conductivity of the nanofluid

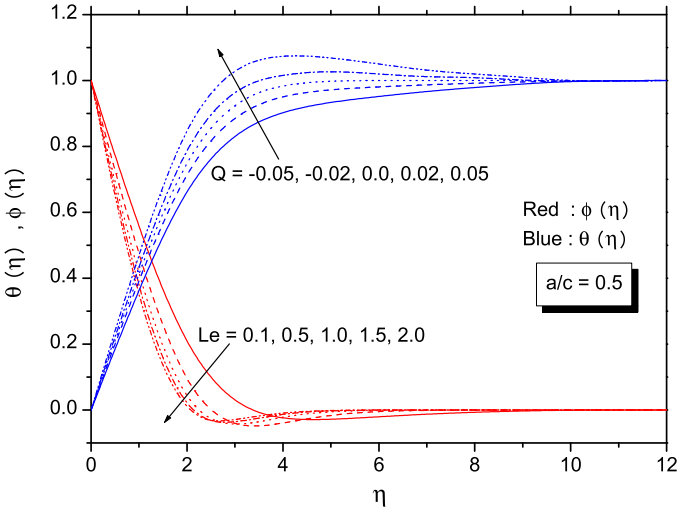

Fig. 17. Effect of Q and *Le* on $\theta(\eta)$ and $\phi(\eta)$ profiles for $a/c = 0.5$ with $\beta = 0.1$, $\lambda = M = 1$, $Nb = Nt = 0.5$, $Pr = 0.72$.

λ^*	Latent heat transfer of the fluid
λ	Reciprocal of magnetic Prandtl number
η	Similarity variable
η_0	Magnetic diffusivity
τ	Ratio of the effective heat capacity of the nanoparticle to that of an ordinary fluid
τ_w	Surface shear stress
ρ_f	Density of the base fluid (kg/m^3)
ρ_p	Density of the nanoparticles (kg/m^3)

Superscript

'	Differentiation with respect to η

References

[1] B.C. Sakiadis, Boundary layer behaviour on continuous solid surface, Amer. Iust. Chem. Eng. J. 7 (1961) 26–28.
[2] L.J. Crane, Flow past a stretching plate, Zeitschrift für Angewandte Mathematik und Physik (ZAMP), 21 (1970) 645–647.
[3] K.-L. Hsiao, Heat and mass mixed convection for MHD viscoelastic fluid past a stretching sheet with Ohmic dissipation, Comm. Nonlin. Sci. Num. Simul. 15 (2010) 1803–1812.
[4] K.-L. Hsiao, Corrigendum to "Heat and mass mixed convection for MHD viscoelastic fluid past a stretching sheet with Ohmic dissipation" [Commun Nonlinear Sci Numer Simulat 15 1803-1812], Comm. Nonlin. Sci. Num. Simul. 28 (13) (2010) 232, doi:10.1016/j.cnsns.2015.04.004.
[5] Z. Liancun, W. Lijuan, Z. Xinxin, Analysis solutions of unsteady flow and heat transfer on a permeable stretching sheet with non uniform heat source/sink, Comm. Nonlin. Sci. Num. Simul. 16 (2011) 731–740.
[6] B.J. Gireesha, B. Mahanthesh, R.S.R. Gorla, P.T. Manjunath, Thermal radiation and Hall effects on boundary layer flow past a non-isothermal stretching surface embedded in porous medium with non-uniform heat source/sink and fluid-particle suspension, Heat Mass Transfer (2015) doi:10.1007/s00231-015-1606-3.
[7] K. Hiemenz, Grenzschicht an einem in den gleichformingen Flussigkeits-strom einge-tauchten graden Kreiszylinder, Dingler's Poly J. 326 (1911) 321–324.
[8] R.S.R. Gorla, Non-Newtonian fluid at a stagnation point in the presence of transverse magnetic field, Mech. Res. Commun. 3 (1976) 1–6.
[9] T.R. Mahapatra, A.S. Gupta, Heat transfer in stagnation point flow towards a stretching sheet, Heat Mass Transfer 38 (2002) 517–521.
[10] R. Nazar, N. Amin, D. Filip, I. Pop, Unsteady boundary layer flow in the region of the stagnation point on a stretching sheet, Int. J. Eng. Sci. 42 (2004) 1241–1253.
[11] A. Ishak, R. Nazar, I. Pop, Mixed convection boundary layers in the stagnation-point flow towards a stretching vertical sheet, Meccanica 41 (2006) 509–518.
[12] H.S. Takhar, A.J. Chamkha, G. Nath, Unsteady axisymmetric stagnation-point flow of a viscous fluid on a cylinder, Int. J. Eng. Sci. 37 (15) (1999) 1943–1957.
[13] G.K. Ramesh, B.J. Gireesha, C.S. Bagewadi, MHD flow of a dusty fluid near the stagnation-point over a permeable stretching sheet with non-uniform source/sink, Int. J. Heat Mass Transfer 55 (2012) 4900–4907.
[14] S.U.S. Choi, Enhancing thermal conductivity of fluids with nanoparticles, ASME: Fluids Engineering Division 231 (1995) 99–105.
[15] W.A. Khan, I. Pop, Boundary layer flow of a nanofluid past a stretching sheet, Int. J. Heat Mass Transfer 53 (2010) 2477–2483.
[16] A.V. Kuznetsov, D.A. Nield, Natural convective boundary-layer flow of a nanofluid past a vertical plate, Int. J. Therm. Sci. 49 (2010) 243–247.
[17] A.J. Chamkha, R.S.R. Gorla, K. Ghodeswar, Non-similar solution for natural convective boundary layer flow over a sphere embedded in a porous medium saturated with a nanofluid, Transport Porous Med. 86 (2011) 13–22.
[18] R.S.R. Gorla, S.M.M.E.L. Kabeir, A.M. Rashad, Heat transfer in the boundary layer on a stretching circular cylinder in a nanofluid, J. Thermophys. Heat Transfer 25 (2011) 183–186.
[19] N. Bachok, A. Ishak, I. Pop, The boundary layers of an unsteady stagnation-point flow in a nanofluid, Int. J. Heat Mass Transfer 55 (2012) 6499–6505.
[20] O.D. Makinde, A. Aziz, Boundary layer flow of a nano fluid past a stretching sheet with a convective boundary condition, Int. J. Therm. Sci. 53 (11) (2011) 2477–2483.
[21] A. Alsaedi, M. Awais, T. Hayat, Effect of heat generation/absorption on stagnation-point flow of nanofluid over a surface with convective boundary conditions, Comm. Nonlin. Sci. Num. Simul. 12 (2012) 4210–4223.
[22] B.J. Gireesha, R.S.R. Gorla, B. Mahanthesh, Effects of suspended nanoparticles on three-dimensional MHD flow, heat and mass transfer of radiating Eyring-Powell fluid over a stretching sheet, J. Nanofluids 4 (2015) 1–11.
[23] H. KaiLong, Nanofluid flow with multimedia physical features for conjugate mixed convection and radiation, Comput. Fluids 104 (2014) 18, doi:10.1016/j.compfluid.2014.08.001.
[24] Z. Chaoli, Z. Liancun, Z. Xinxin, C. Goong, MHD flow and radiation heat transfer of nanofluids in porous media with variable surface heat flux and chemical reaction, Appl. Math. Model. 39 (2015) 165–181.
[25] Z. Liancun, Z. Chaoli, Z. Xinxin, Z. Junhong, Flow and radiation heat transfer of a nanofluid over a stretching sheet with velocity slip and temperature jump in porous medium, J. Frankl. Inst. 350 (2013) 929–1334.
[26] B.J. Gireesha, B. Mahanthesh, R.S.R. Gorla, Suspended particle effect on nanofluid boundary layer flow past a stretching surface, J. Nanofluids 3 (2014) 1–11.
[27] E.M. Epstein, D.H. Cho, Melting heat transfer in steady laminar flow over a flat plate, J. Heat Transfer 98 (1976) 531–533.
[28] M. Kazmierczak, D. Poulikakos, I. Pop, Melting from a flat plate embedded in a porous medium in the presence of steady convection, Numer. Heat Transfer 10 (1986) 571–581.
[29] R.S.R. Gorla, M.A. Mansour, I.A. Hussanien, A.Y. Bakier, Mixed convection effect on melting from a vertical plate, Transport Porous Med. 36 (1999) 245–254.
[30] N. Bachock, A. Ishak, I. Pop, Melting heat transfer in boundary layer stagnation-point flow towards a stretching/shrinking sheet, Phys. Lett. A 374 (2010) 4075–4079.
[31] Y. Koshiba, T. Matsushita, M. Ishikawa, Influence of induced magnetic field on large-scale pulsed MHD generator, 33rd Plasmadynamics and Lasers Conference, AIAA (2002) 2002–2145.
[32] M. Kumari, H.S. Takhar, G. Nath, MHD flow and heat transfer over a stretching surface with prescribed wall temperature or heat flux, Warme Stoffubertrag 25 (6) (1990) 331–336.
[33] H.S. Takhar, A.J. Chamkha, G. Nath, Unsteady flow and heat transfer on a semi-infinite flat plate with an aligned magnetic field, Int. J. Eng. Sci. 37 (1999) 1723–1736.
[34] O.A. Beg, A.Y. Bakier, V.R. Prasad, J. Zueco, S.K. Ghosh, Non-similar, laminar, steady, electrically conducting forced convection liquid metal boundary layer flow with induced magnetic field effects, Int. J. Therm. Sci. 48 (2009) 1596–1606.
[35] S.K. Ghosh, O.A. Beg, J. Zueco, Hydromagnetic free convection flow with induced magnetic field effects, Meccanica 45 (2010) 175–185.
[36] Z. Liancun, N. Jiajia, Z. Xinxin, G. Yingtao, MHD flow and heat transfer over a porous shrinking surface with velocity slip and temperature jump, Math. Comput. Model. 56 (2012) 133–144.
[37] F.M. Ali, R. Nazar, N.M. Arifin, I. Pop, MHD boundary layer flow and heat transfer over a stretching sheet with induced magnetic field, Heat Mass Transfer 47 (2011) 155–162.
[38] F.M. Ali, R. Nazar, N.M. Arifin, I. Pop, MHD stagnation-point flow and heat transfer towards stretching sheet with induced magnetic field, Appl. Math. Mech. – Engl. Ed. 32 (4) (2011) 409–418.